Supporting Information

2D-3D Co-conduction Effect in PEO-based All-Solid-State Battery for Long Cycle Stability

Hao He, Yuan Chai, Xinlong Zhang, PenghuiShi, JinchenFan[a,b], QunjieXu[a,b]*, YulinMin[a,b]**

[a]*Shanghai Key Laboratory of Materials Protection and Advanced Materials Electric Power, Shanghai University of Electric Power, Shanghai 200090, P. R. China*

[b]*Shanghai Institute of Pollution Control and Ecological Security, Shanghai200092, P.R. China*

E-mail: Jinchen.fan@shiep.edu.cn; xuqunjie@shiep.edu.cn; ahaqmylin@126.com;

Experimental Methods

Preparation of LLGO nanoparticles:

The LLGO particles were synthesized via a high temperature solid-phase method. The amounts of lithium carbonate (Li_2CO_3), lanthanum trioxide (La_2O_3) and Gallium Oxide (Ga_2O_3) were calculated for $Li_{19}La_{36}Ga_7O_{74}$. The raw materials were mixed by ball milling in isopropanol at a rotation speed of 600 rpm for 20h. The resulting mixture was dried at 60 ºC and then continuously sintered at 850 ºC for 6 h and 900 ºC for 4 h with a heating rate of 2 ºC min^{-1}. And the obtained LLGO was grinded in mortar and then was ball milled with Yttria-stabilized zirconia (YSZ) ball (with a diameter of 1 mm) for 12 h to obtain nanoparticles.

Preparation of solid composite electrolytes (SCEs):

PEO (Mw ~ 600,000) and lithium bis(trifluoromethanesulfonyl)imide (LiTFSI) were dried at 60 ℃ in vacuum for 24 h before use. The SCEs were prepared by first dissolving PEO and LiTFSI in anhydrous acetonitrile with EO/Li molar ratio of 8:1. Different amount of LLGO powder was added into the solution. The solution was sealed in a glass vial and stirred at 40 ℃ for 24 h and then cast onto a PTFE dish. After drying at 50 ℃ for 24 h in vacuum, the SCEs was obtained and stored in an Ar–filled glove box (H_2O < 1 ppm and O_2 < 1 ppm) for later use. The SCEs was punched with a diameter of 16 mm.

Preparation of LLGO solid electrolyte pellet:

The LLGO pellet prepared by solid-phase reaction was cold-pressed through a tablet press at a pressure of 60 MPa.

The ionic conductivity (σ) of LLGO can be calculated by Equation 1:

$$\sigma = d / Re \cdot S \quad (1)$$

Where σ is the total ionic conductivity, d is the thickness, Re is the total resistance, and S is the cross-sectional area.

Preparation of all-solid-state batteries (ASSBs):

The ASSBs were assembled in 2032-type coin cells by contacting lithium metal anode, the as-prepared SCEs and $LiFePO_4$ or NCM cathode. The cathode was composed of 80 wt% $LiFePO_4$ or NCM, 10 wt% carbon black, and 10 wt%

polyvinylidene fluoride (PVDF) binder. The cathode composite was added into N-methyl-2-pyrrolidone (NMP) and then coated on aluminum substrate. Subsequently, the NMP was removed at 60 °C under vacuum, and the electrode was punched with a diameter of 14 mm. The areal mass loading of LFP was 1.4-1.8 mg cm^{-2}. The batteries were sealed in an Ar-filled glove box and then housed at 60 °C for 10 h to reduce the interfacial impedance between electrode and electrolyte. The cathode material, PLG electrolyte and lithium metal foil were stacked into a rectangle with an area of 9×4 cm, and assembled into a soft- package lithium-ion battery in an Ar-filled glove box. The areal mass loading of LFP was about 2 mg cm^{-2}. The charge-discharge rates were calculated with respect to the theoretical capacities of $LiFePO_4$ (170 $mAhg^{-1}$) and NCM (270 $mAhg^{-1}$), respectively.

Characterization of the solid composite electrolytes (SCEs) :

The product was characterized by using the XRD Bruker D8 advance at 40 KV/40 mA with Cu K radiation (λ=0.154 nm). The morphology of the samples was investigated by using FESEM (JEM-7800F). Transmission electron microscopy (TEM) images were obtained on the JEOL JEM-2100F with Cs correction. Elemental mapping was conducted on an energy-dispersive X-ray spectroscopy (EDS). The particle size distribution diagrams of LLGO and LLZO powder samples were obtained by Shimadzu SALD-2201 laser particle size analyzer. Differential scanning calorimetry (DSC) were carried out on a NETZSCH DSC 200F3 analyzer in N_2 in the temperature range of -90 – -20 °C at a heating rate of 5 °C min^{-1}. FTIR spectra were obtained on PerkinElmer FTIR spectrometer in the range of 4000–400 cm^{-1}. Raman spectrum was measured by Horiba Raman analyzer in the range of 200–1300 cm^{-1}. TGA and were carried out on a NETZSCH STA 409 PC/PG analyzer in N_2 in the temperature range of 25 -700 °C at a heating rate of 5 °C min^{-1}. The tensile properties of SCEs are measured by a SANS universal testing machine at a speed of 10mm/min. The width of the tensile specimen is 5mm and the thickness is 0.2mm.

Electrochemical impedance spectroscopy (EIS) measurements were conducted on Chenhua electrochemical workstation with an AC amplitude of 10 mV and a frequency range from 1 MHz to 0.1 Hz. The ionic conductivity of the SCEs was tested using a symmetric SS|SCEs|SS (SS =stainless steel) from 25℃ to 80 ℃. The ionic conductivity, σ, can be evaluated by equation 2:

$$\sigma = L/RS \quad (2)$$

Where R, L and S are the resistance, thickness and area of the SCEs, respectively.

A Li|SCEs|Li battery was assembled to estimate the transference number of Li ions (t Li^+) through the chronoamperometry test. t Li^+ can be deduced by equation 3:

$$t\ Li^+ = I_{ss}/I_0 \times (V - I_0R_0)/(V - I_{SS}R_{SS}) \quad (3)$$

Where V, I_0, I_{ss}, R_0 and R_{ss} are the applied voltage, initial and steady-state currents and the impedance before and after the chronoamperometry test.

Linear sweep voltammetry was conducted with Li|SCEs|SS battery at 60 ℃.

Cyclic voltammetry (CV) study was evaluated by electrochemical workstations at voltage ranges of 2.5-4.0 V with a scan rate of 0.1 mVs^{-1} at 60 ℃. Galvanostatic charge/discharge curves and rate performance tests were performed on a LAND CT2001 test system. The stability of the SCEs against Li metal was evaluated by a symmetrical Li|SCEs|Li cell at different current densities.

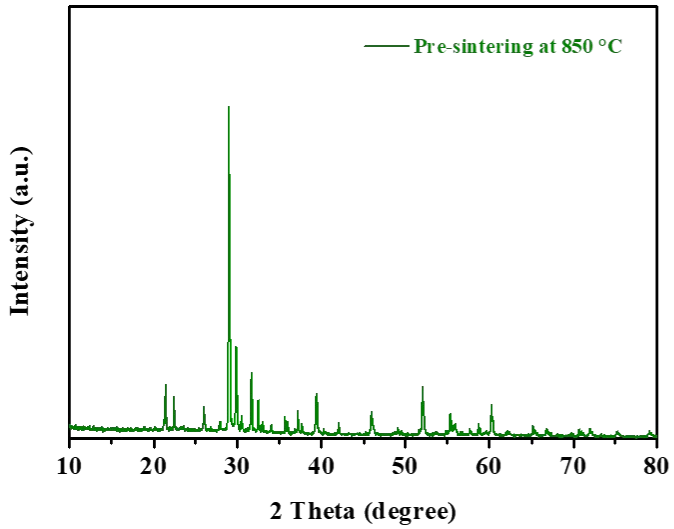

Figure S1.XRD pattern of LLGO precursor particles prepared by pre-sintering at 850°C.

Figure S2. Digital images of electrolyte powders and pellets synthesized at 850℃ and 900℃, respectively.

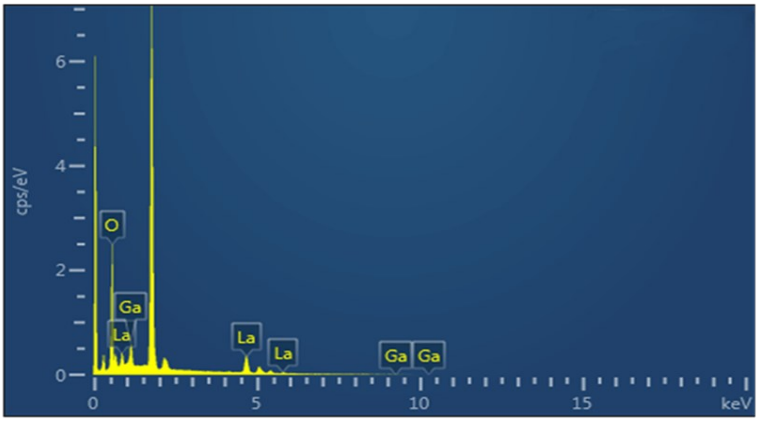

Element	Apparent concentration	K ratio	wt%	wt% Sigma	Atomic percentage
O	15.61	0.13679	20.34	0.46	66.62
Ga	4.22	0.03917	8.92	0.44	6.70
La	55.81	0.50076	70.74	0.67	26.68

Figure S3. The EDX element composition of LLGO particles in Figure 1b.

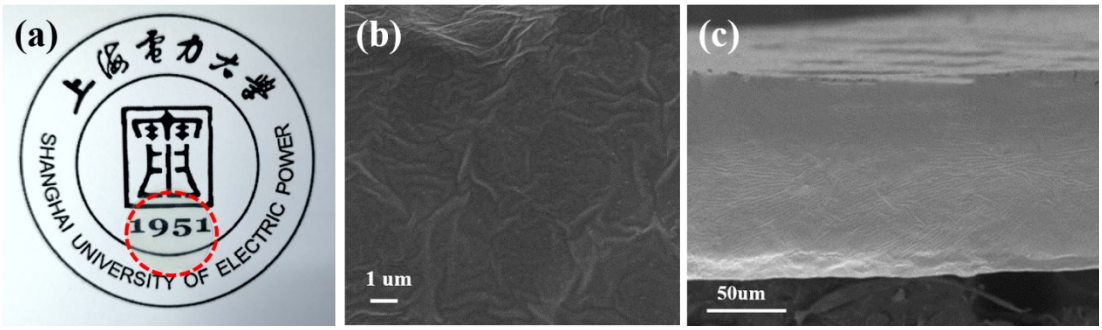

Figure S4. (a) Optical image of PL. (b) SEM image(top) of PL. (c) SEM image(cross section) of PL.

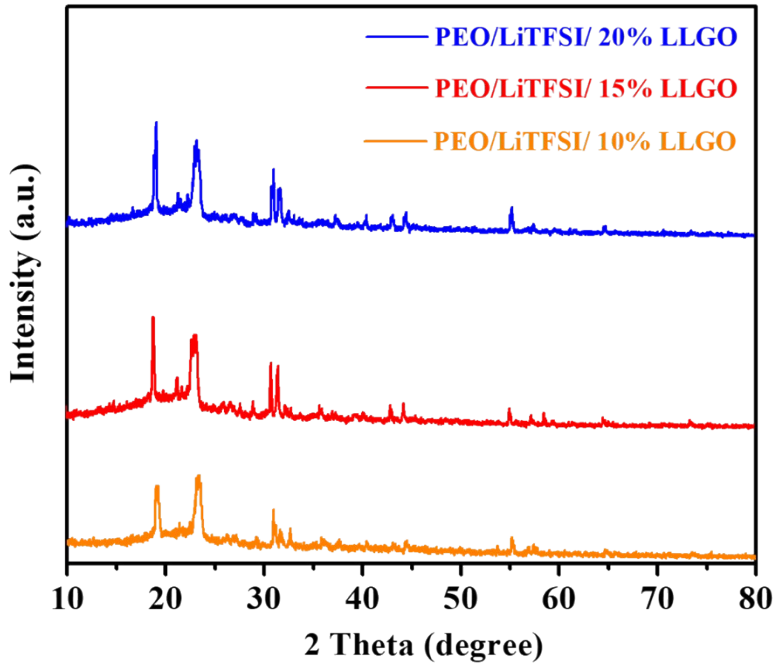

Figure S5. XRD patterns of PLG with different mass fractions of LLGO.

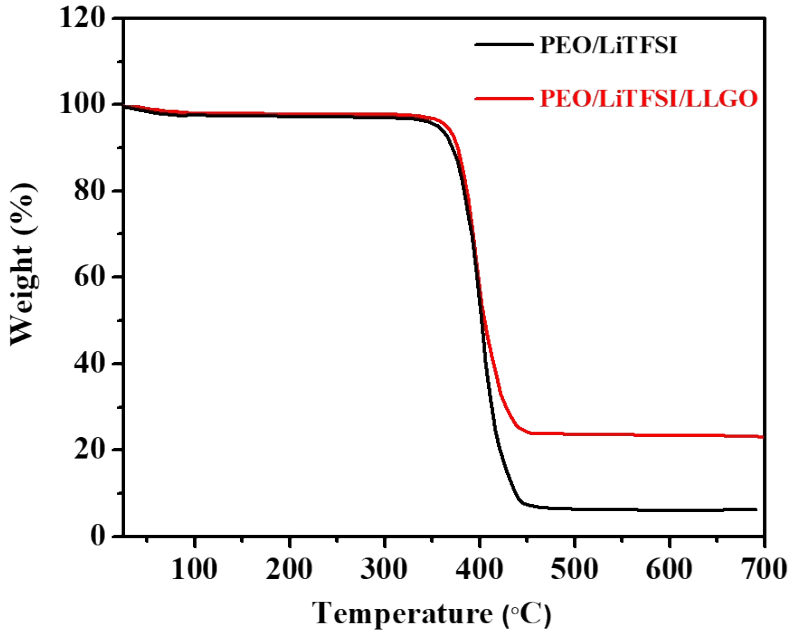

Figure S6. TGA curves of PL and PLG.

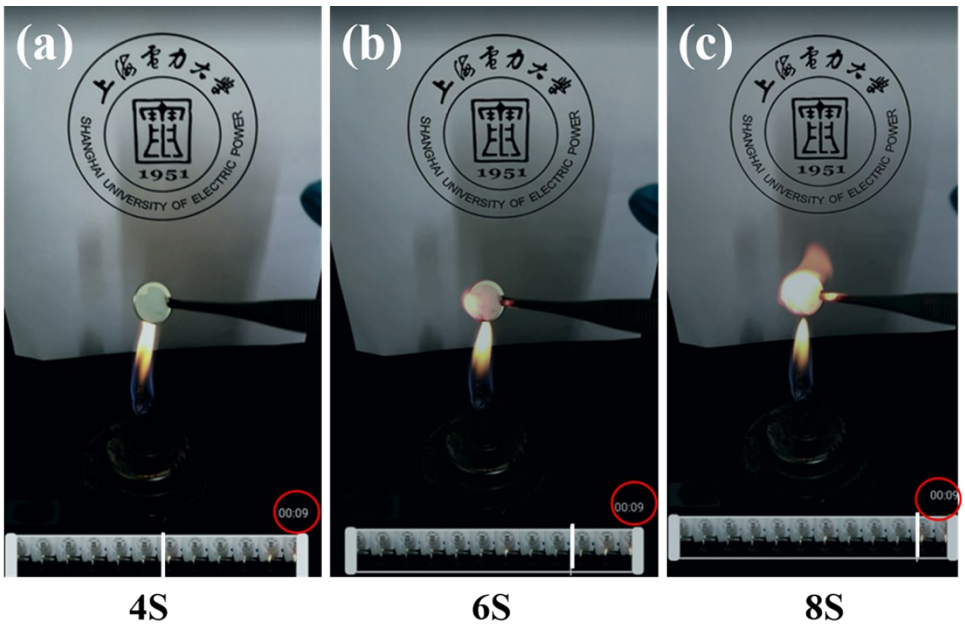

Figure S7. Combustion tests of PL.

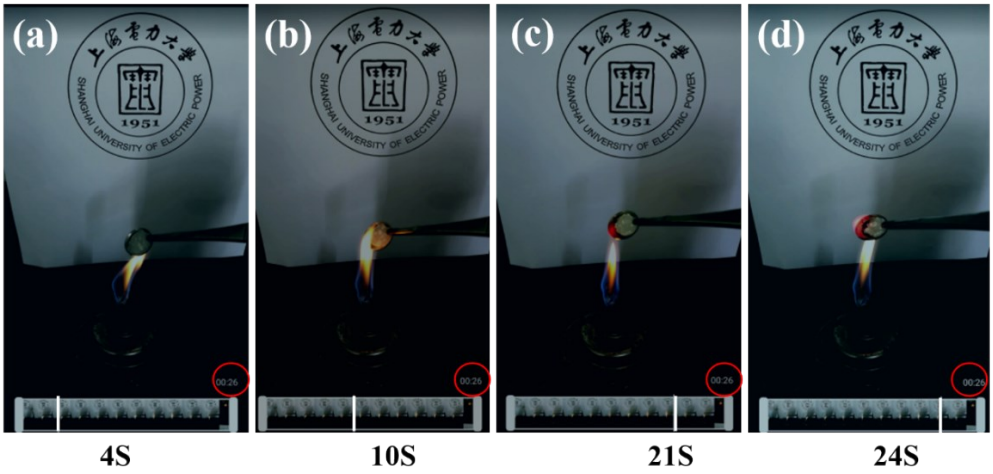

Figure S8. Combustion tests of PLG.

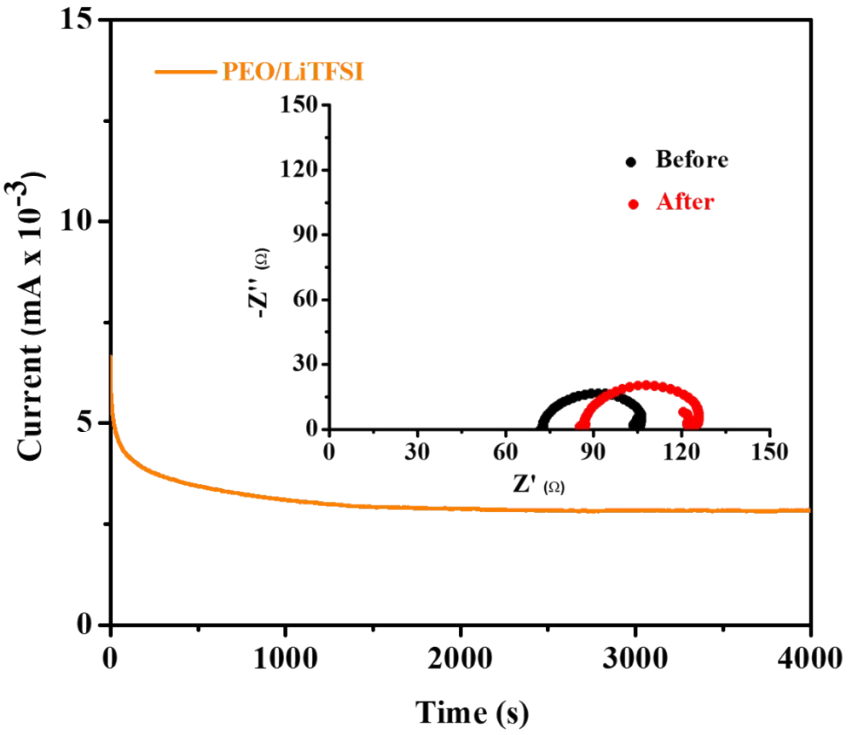

Figure S9. The chronoamperometry curves of PL at a potential step of 10 mV at 60 ℃. Inset: AC impedance spectra of the same cell before and after polarization.

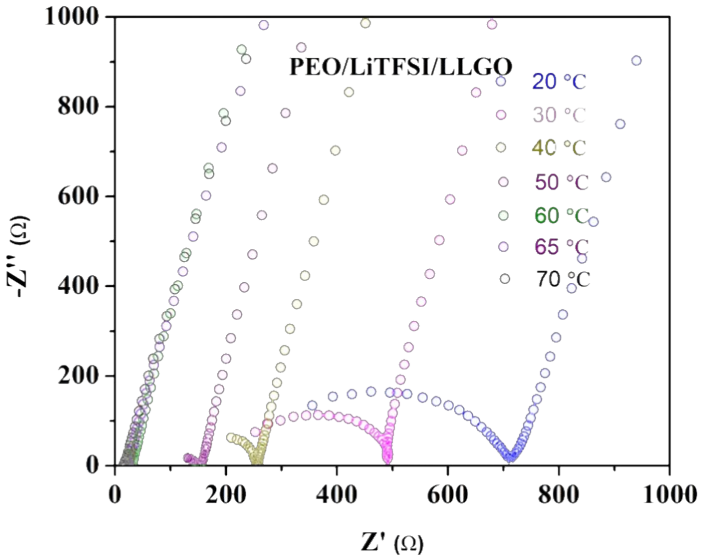

Figure S10. Impedance spectra of PLG at different temperatures.

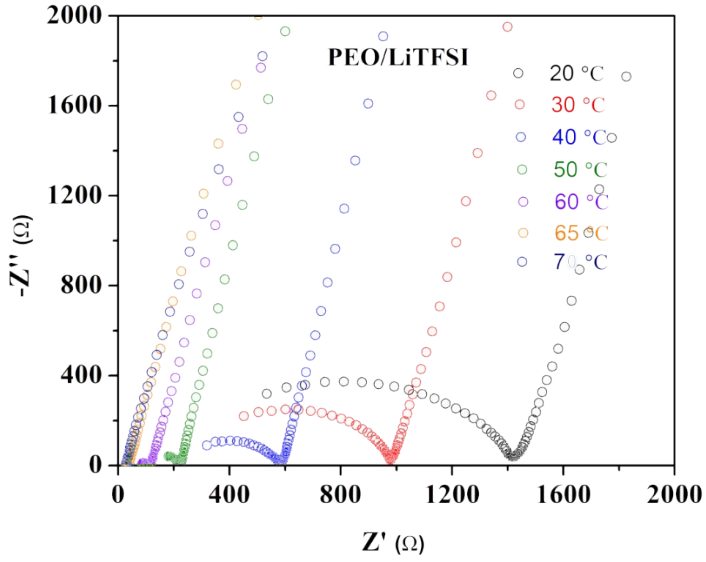

Figure S11. Impedance spectrum of PL at different temperatures.

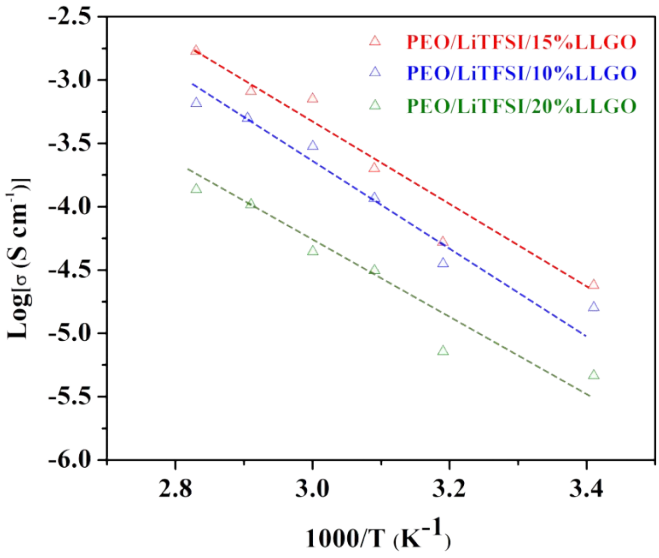

Figure S12. Arrhenius plots of Li^+ conductivities of the PLG membranes with different content of LLGO.

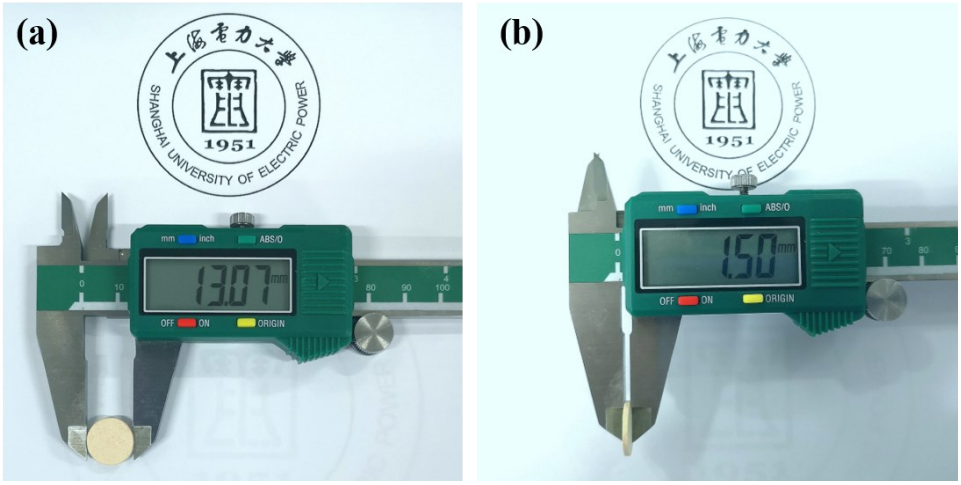

Figure S13. Digital photos of LLGO pellet diameter and thickness.

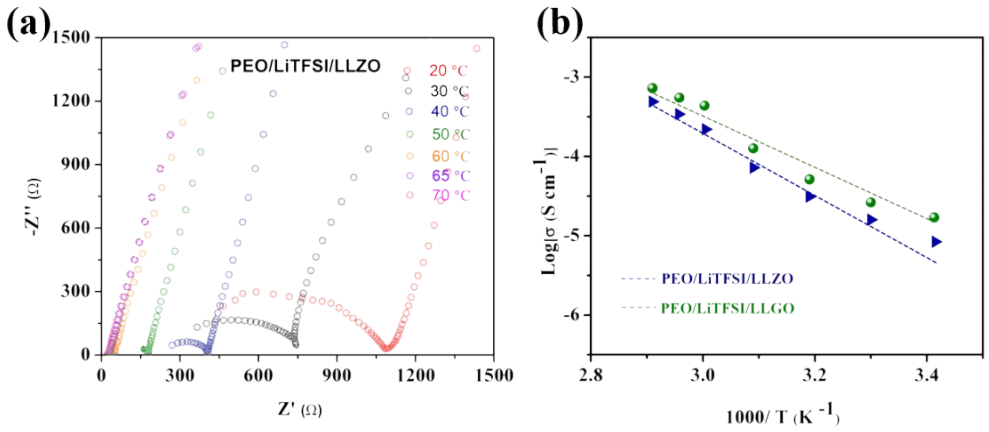

Figure S14. (a) Impedance spectrum of PLZ at different temperatures. (b) Arrhenius plots of Li^+ conductivities of the PLZ, PLG composite electrolytes.

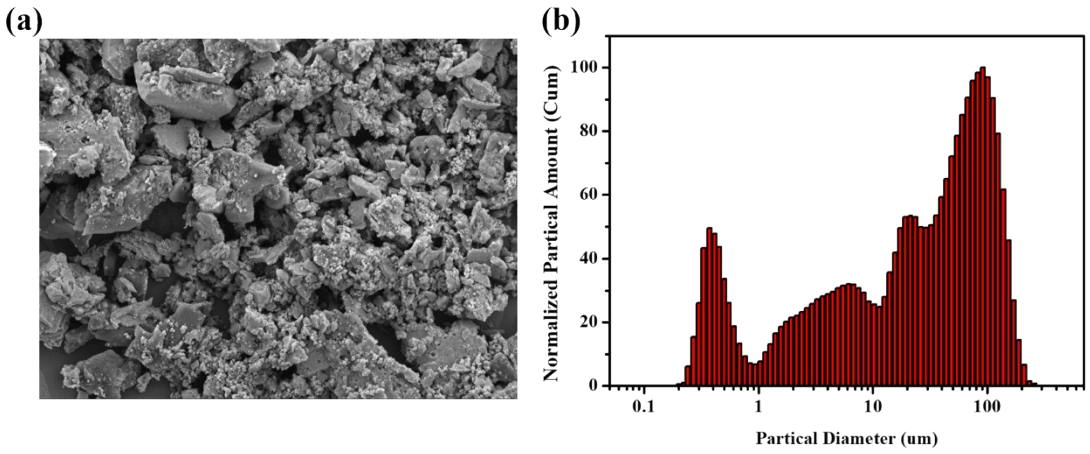

Figure S15. (a) SEM image of LLZO particles. (b) The particle size distributions of LLZO.

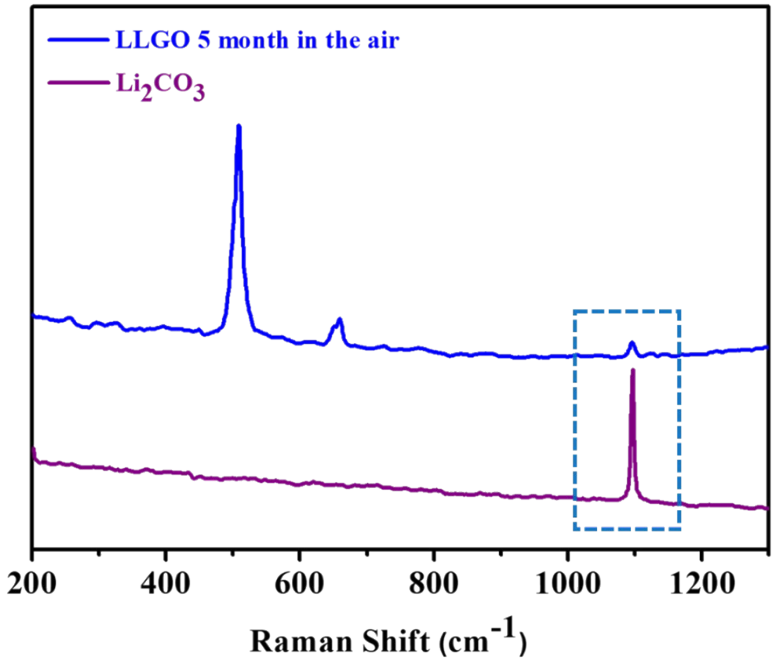

Figure S16. Raman spectrum of LLGO particle held in air for 5 month and Li_2CO_3 to confirm the chemical stability of LLGO.

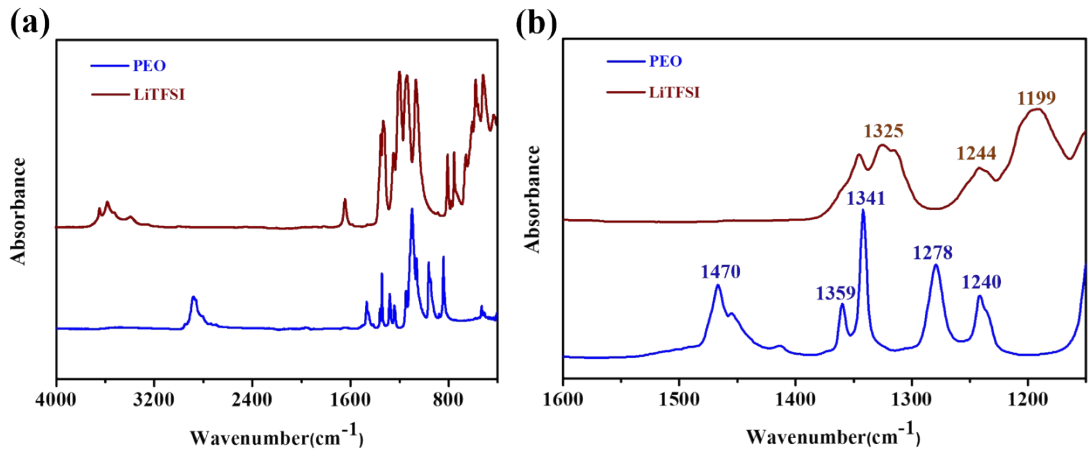

Figure S17. FTIR spectra for PEO and LiTFSI at (a) 4000–400 cm^{-1} and (b) 1600–1150 cm^{-1}.

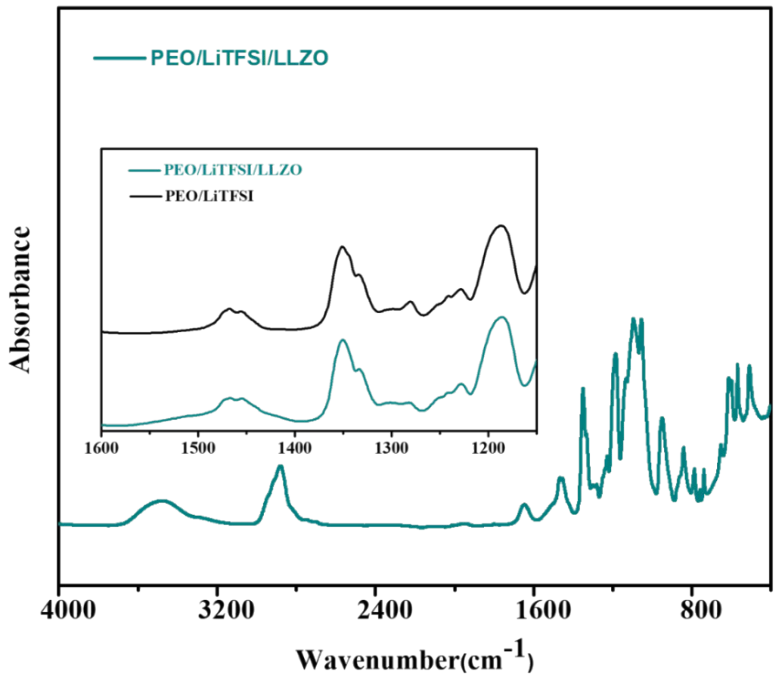

Figure S18. FTIR spectra for PLZ at 4000–400 cm^{-1}. Inset: FTIR spectra for PL film and PLZ film at 1600–1150 cm^{-1}

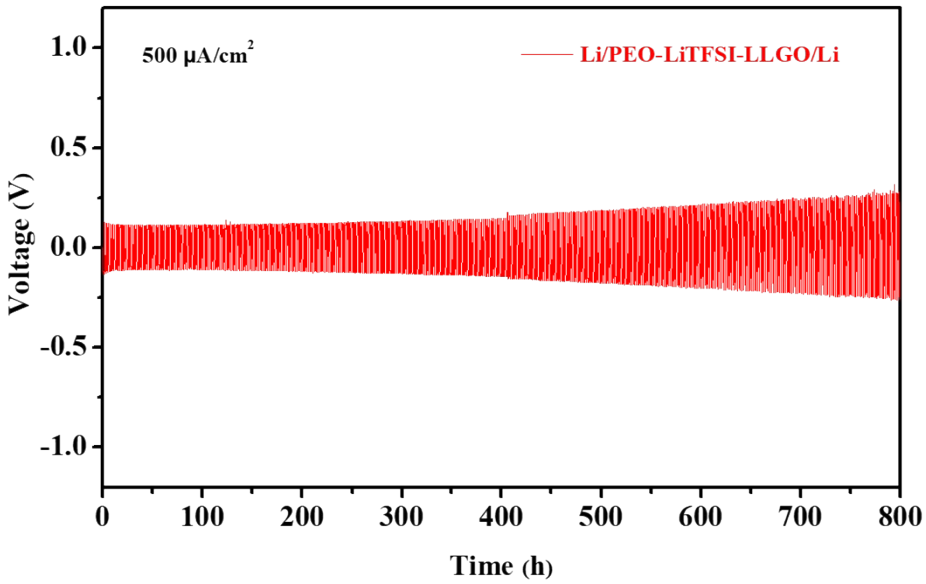

Figure S19. Voltage profile of the continued lithium plating/stripping cycling of Li|PLG|Li battery with a current density of 500 μA/cm^2 at 60°C. The plating Li capacity is 0.5 mAh/cm^2 per cycle.

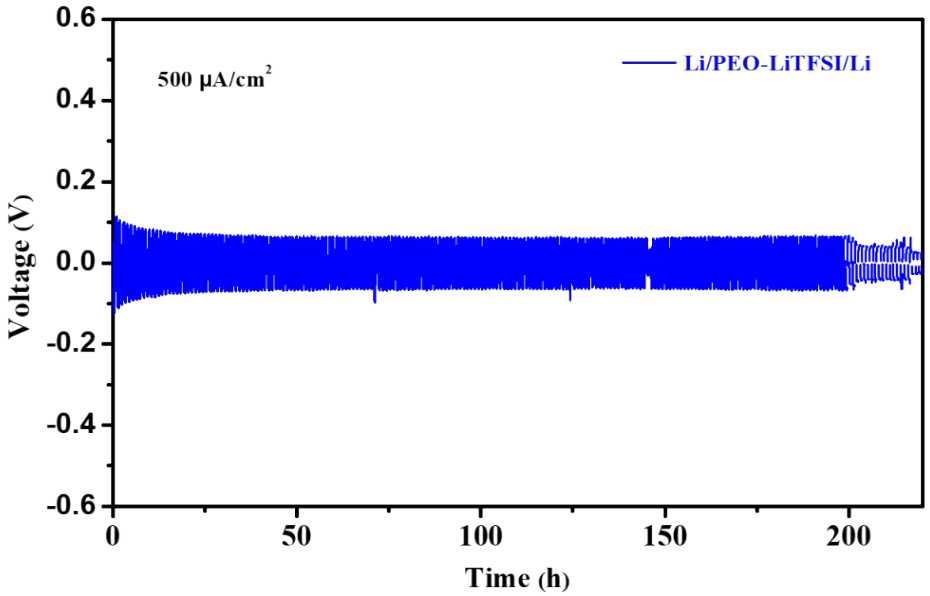

Figure S20. Voltage profile of the continued lithium plating/stripping cycling of Li|PL|Li cell with a current density of 500 μA/cm^2 at 60 °C. The plating Li capacity is 0.5 mAh/cm^2 per cycle.

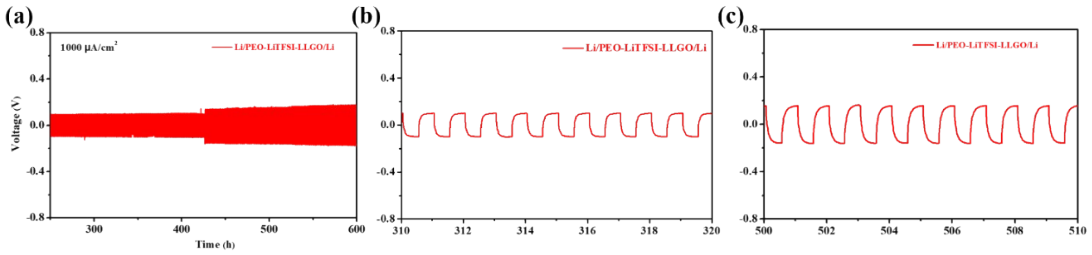

Figure S21. Voltage profile of the continued lithium plating/stripping cycling of Li|PLG|Li cell with a current density of 1000 μA/cm^2 at 60 °C and 65 °C. The plating Li capacity is 1 mAh/cm^2 per cycle.

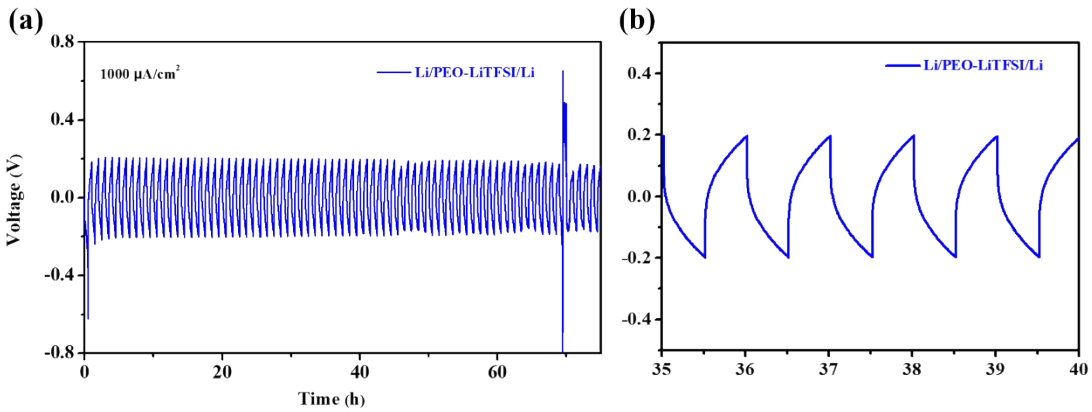

Figure S22. Voltage profile of the continued lithium plating/stripping cycling of Li|PL|Li cell with a current density of 1000 μA/cm^2 at 60 °C. The plating Li capacity is 1 mAh/cm^2 per cycle.

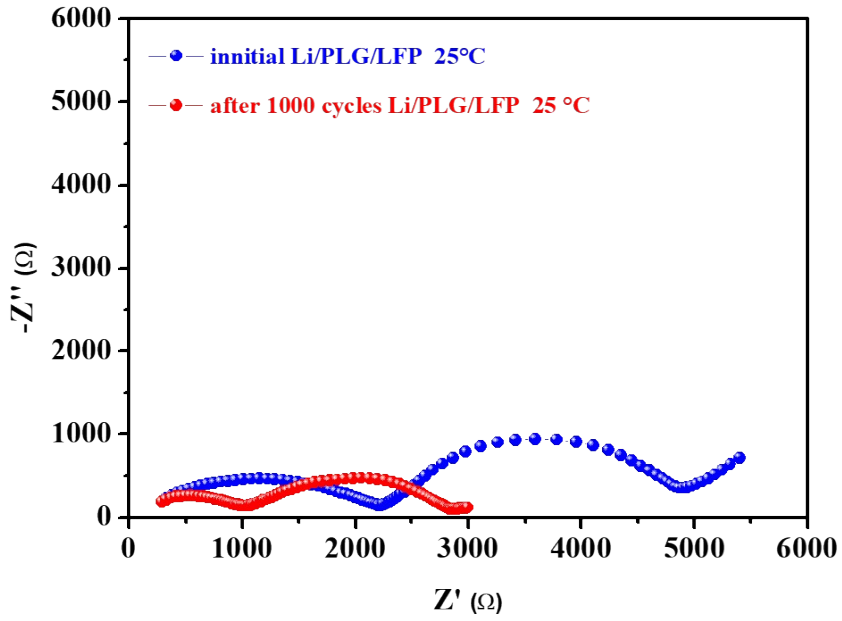

Figure S23. Nyquist profiles of innitial Li|PLG|LFP and Li|PLG|LFP after cycling for 1000 cycles at 25 ℃.

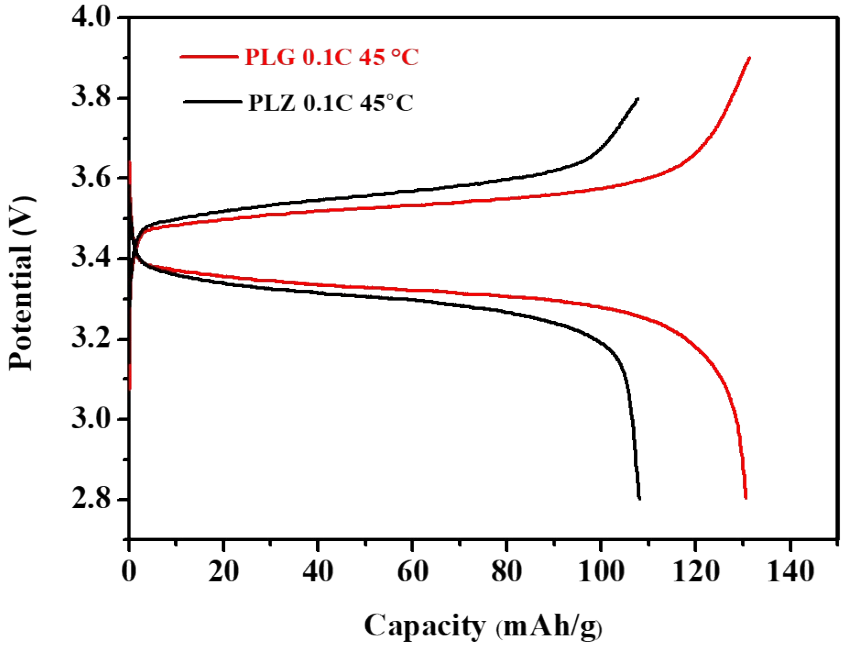

Figure S24. Charge–discharge voltage profiles of LFP|PLG|Li, LFP|PLZ|Li batteries at 0.1C under 45°C.

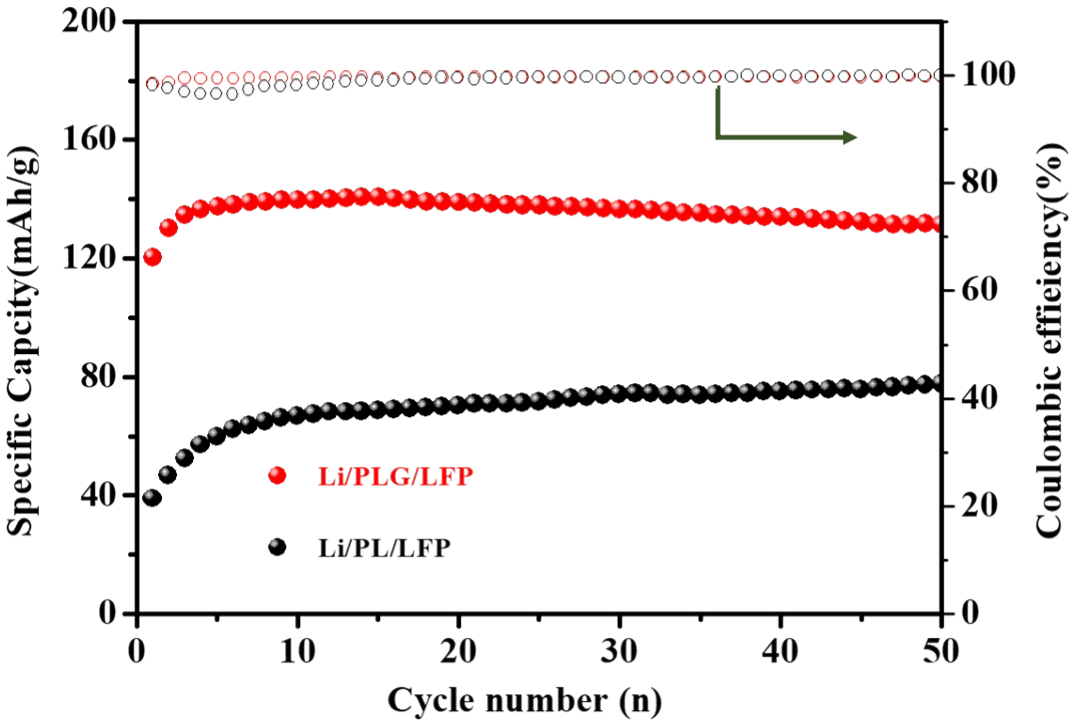

Figure S25. Cycling performances of LFP|PLG|Li, LFP|PL|Li at 0.1 C and 45 °C.

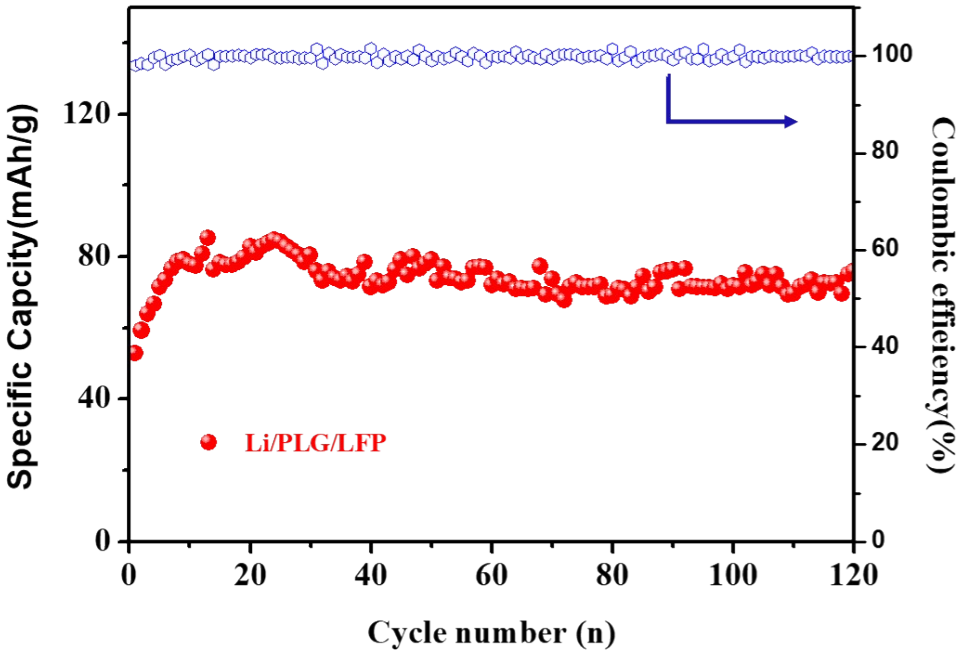

Figure S26. Cycling performances of LFP|PLG|Li at 0.1 C and 25 °C.

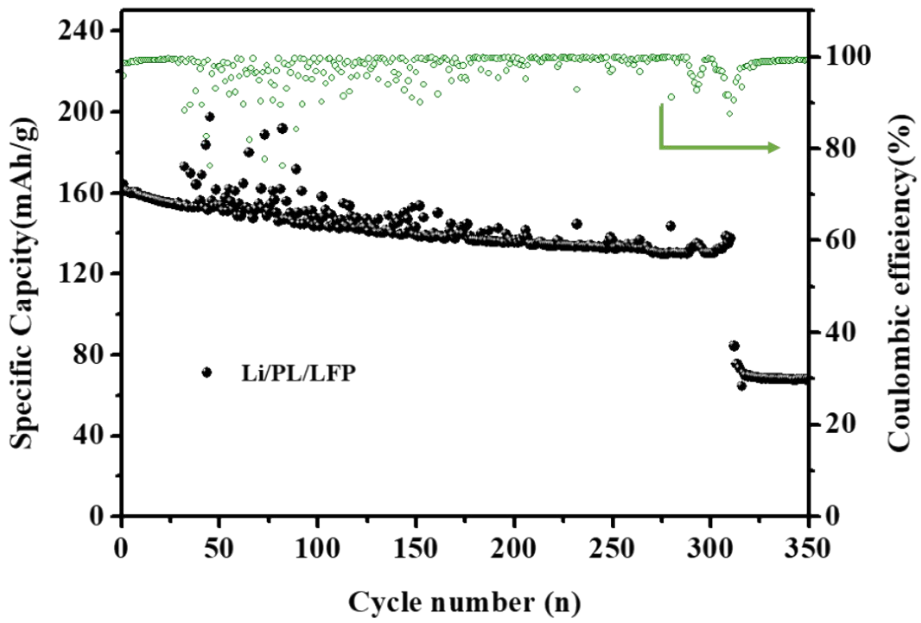

Figure S27. Cycling performances of LFP|PL|Li at 0.2 C and 60 °C.

Solid electrolytes	Working temperature	Discharge capacities	Rate capacities	Ref.
PEO-Al_2O_3-LITFSl	50 ℃	169 mAh g-1 (0.05C)	36(1C)	1
	30 ℃	42 mAh g^{-1} (0.05C)	/	
PEO-$MgAl_2O_4$-LiPF6	70 ℃	110 mAh g^{-1} after 100 cycles under 1C	/	2
PEO-LGPS-LiTFSI	60 ℃	137 mAh g^{-1} after 50 cycles under 0.5C	99(1C)	3
PEO-LLZTO-LiTFSI	60 ℃	135 mAh g^{-1} after 100cycles under 0.1C	/	4
PEO-LAGP-$LiClO_4$	55 ℃	121.5 mAh g^{-1} after 100cycles under 0.2C	95(2C)	5
PEO-LLZO-LiTFSI	60 ℃	121 mAh g^{-1} after 100cycles under 0.5C	100.2(1C)	6
(LiTFSI-Al_2O_3-CPEO)-LLZT	65 ℃	100 mAh g^{-1} after 100cycles under 160 uA cm^{-2}	/	7

PEO-LLTO	65 ℃	125 mAh g^{-1} after 50cycles under 0.05C	/	8
PEO-LLZO nanofiber-LiTFSI	/	/	/	9
PEO-PI-LiTFSI	60 ℃	110 mAh g^{-1} after 300cycles under 0.5C	124(1C)	10
PEO-$Mg_2B_2O_5$ nanowire-LiTFSI	50 ℃	120 mAh g^{-1} after 230 cycles under 1C	72(2C)	11
PEO-5wt%ANF-LiTFSI	40 ℃	135 mAh g^{-1} after 100 cycles under 0.4C	95(0.5C)	12
PEO-Ca/CeO_2-LiTFSI	60 ℃	100 mAh g^{-1} after 100 cycles under 1C	100（2C)	13
PEO-SiO_2 aerogel-LiTFSI	18 ℃	90 mAh g^{-1} after 200 cycles under 0.5C	170(0.4C)65℃	14
PEO-SiO_2-LiTFSI	90 ℃	105 mAh g^{-1} after 65 cycles under 1C	105(1C)	15
PEO-MnO_2-LiTFSI	60 ℃	110 mAh g^{-1} after 300 cycles under 0.5C	86.6(1C)	16
PEO-h/BN-LiTFSI	60 ℃	139.5 mAh g^{-1} after 50 cycles under 0.5C 143.3 mAh g^{-1} after 140 cycles under 0.2C	95(1C)	17
PEO-LLZO particles-LiiTFSI	60 ℃	107 mAh g^{-1} after 200 cycles under 0.1 C	77.8(2C)	18
PEO-LAGP-LiTFSI	60 ℃	100 mAh g^{-1} after 50 cycles under 1 C	110(1C)	19
PEO-10 wt% LLZTO-LITFSI	55 ℃	127 mAh g^{-1} after 200 cycles under 0.2 C	44.5(3C)	20
PEO-LATP/PAN nanofiber -LiTFSI	60 ℃	144 mAh g^{-1} after 100 cycles under 0.2 C	90（2C)	21
PAN-LLTO nanowires -$LiClO_4$	/	/	/	22
PEO-LLTO nanowires -LiTFSI	/	/	/	23
PEO-LLGO particles-LiTFSI	60 ℃	120 mAh g^{-1} after 400 cycles under 0.2 C 100 mAh g^{-1} after 1000 cycles under 0.5 C 102 mAh g^{-1} after 250 cycles under 1 C	130(1C)	**This work**
	45 ℃	110 mAh g^{-1} after 130 cycles under 0.2 C	/□	
	25 ℃	80 mAh g^{-1} after 120 cycles under 0.1 C	/□	

Table S1. The electrochemical performance of Li metal batteries using different solid electrolytes.

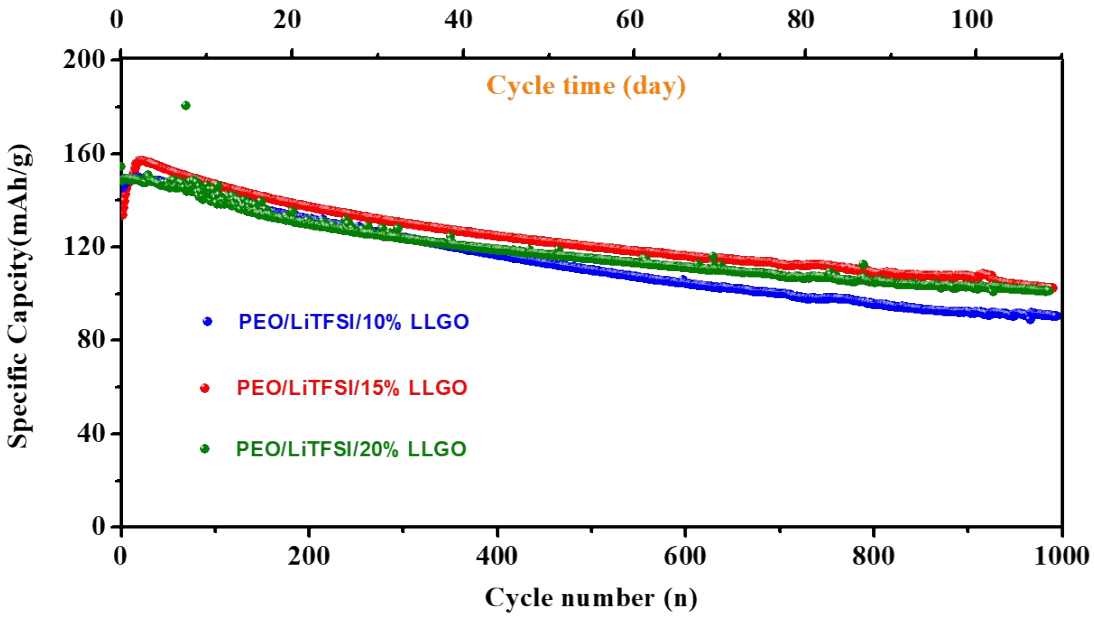

Figure S28. Cycling performances of LFP|PLG|Li with different mass fractions of LLGO at 1 C and 60 °C.

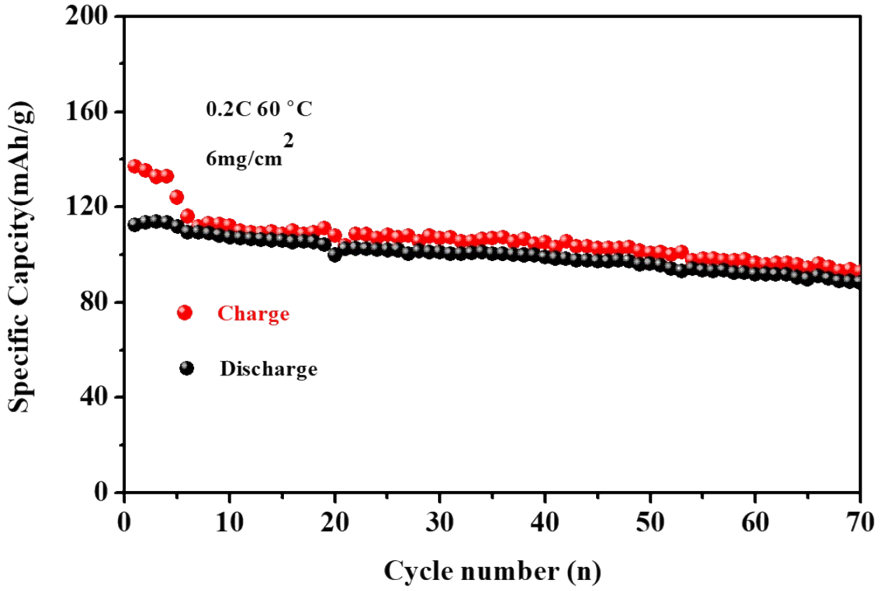

Figure S29. Cycling performances of LFP|PLG|Li at 0.2 C and 60 °C. The positive electrode active material loading is 6 mg/cm^2.

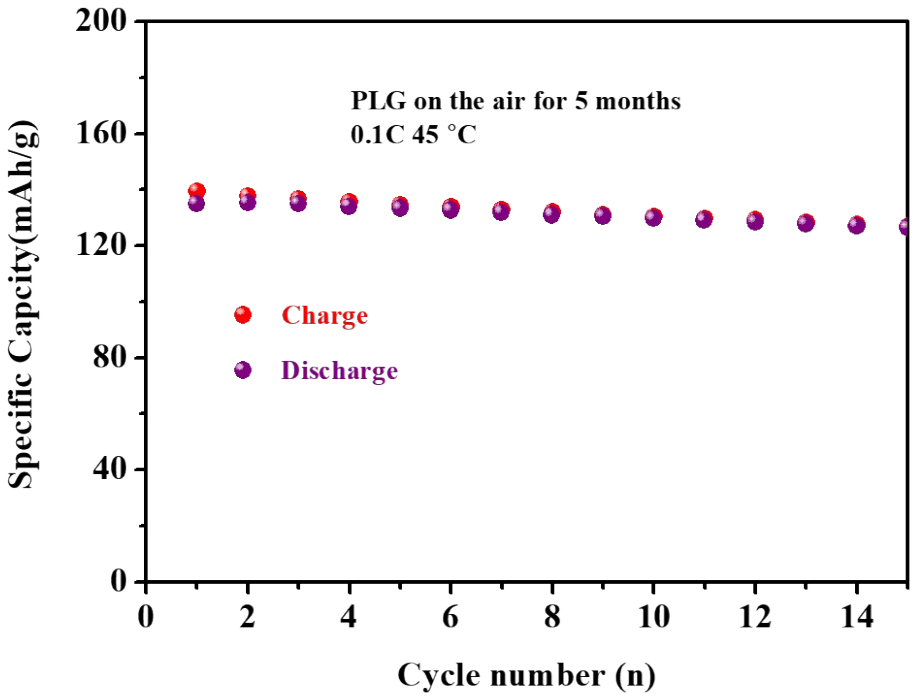

Figure S30. Cycling performances of LFP|PLG|Li at 0.1 C and 45 °C. The PLG SCEs was held in the air for 5 months.

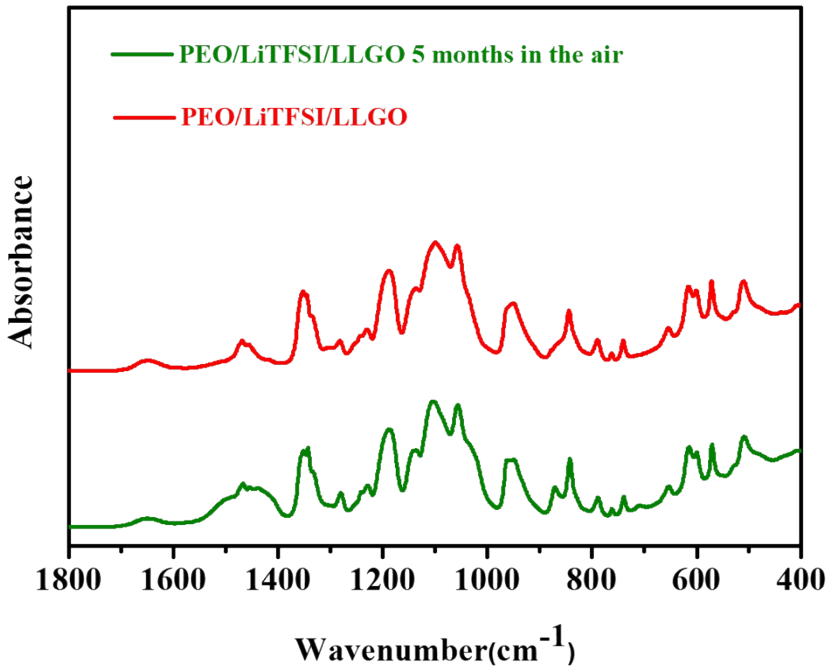

Figure S31. FTIR spectra for PLG and PLG SCEs held in the air for 5 months at 4000–400 cm^{-1}.

References:

1. Chen, X.; He, W.; Ding, L.-X.; Wang, S.; Wang, H., Enhancing interfacial contact in all solid state batteries with a cathode-supported solid electrolyte membrane framework. *Energy & Environmental Science* **2019,** *12* (3), 938-944.
2. Angulakshmi, N.; Nahm, K. S.; Nair, J. R.; Gerbaldi, C.; Bongiovanni, R.; Penazzi, N.; Stephan, A. M., Cycling profile of $MgAl_2O_4$-incorporated composite electrolytes composed of PEO and $LiPF_6$ for lithium polymer batteries. *Electrochimica Acta* **2013,** *90*, 179-185.
3. Zhao, Y.; Wu, C.; Peng, G.; Chen, X.; Yao, X.; Bai, Y.; Wu, F.; Chen, S.; Xu, X., A new solid polymer electrolyte incorporating $Li_{10}GeP_2S_{12}$ into a polyethylene oxide matrix for all-solid-state lithium batteries. *Journal of Power Sources* **2016,** *301*, 47-53.
4. Zhao, C. Z.; Zhang, X. Q.; Cheng, X. B.; Zhang, R.; Xu, R.; Chen, P. Y.; Peng, H. J.; Huang, J. Q.; Zhang, Q., An anion-immobilized composite electrolyte for dendrite-free lithium metal anodes. *Proc Natl Acad Sci USA* **2017,** *114* (42), 11069-11074.
5. Jung, Y.-C.; Lee, S.-M.; Choi, J.-H.; Jang, S. S.; Kim, D.-W., All Solid-State Lithium Batteries Assembled with Hybrid Solid Electrolytes. *Journal of The Electrochemical Society* **2015,** *162* (4), A704-A710.
6. Chen, F.; Yang, D.; Zha, W.; Zhu, B.; Zhang, Y.; Li, J.; Gu, Y.; Shen, Q.; Zhang, L.; Sadoway, D. R., Solid polymer electrolytes incorporating cubic $Li_7La_3Zr_2O_{12}$ for all-solid-state lithium rechargeable batteries. *Electrochimica Acta* **2017,** *258*, 1106-1114.
7. Li, Y.; Xu, B.; Xu, H.; Duan, H.; Lu, X.; Xin, S.; Zhou, W.; Xue, L.; Fu, G.; Manthiram, A.; Goodenough, J. B., Hybrid Polymer/Garnet Electrolyte with a Small Interfacial Resistance for Lithium-Ion Batteries. *Angew Chem Int Ed Engl* **2017,** *56* (3), 753-756.
8. Jiang, Z.; Xie, H.; Wang, S.; Song, X.; Yao, X.; Wang, H., Perovskite Membranes with Vertically Aligned Microchannels for All-Solid-State Lithium Batteries. *Advanced Energy Materials* **2018,** *8* (27).
9. Fu, K. K.; Gong, Y.; Dai, J.; Gong, A.; Han, X.; Yao, Y.; Wang, C.; Wang, Y.; Chen, Y.; Yan, C.; Li, Y.; Wachsman, E. D.; Hu, L., Flexible, solid-state, ion-conducting membrane with 3D garnet nanofiber networks for lithium batteries. *Proc Natl Acad Sci U S A* **2016,** *113* (26), 7094-9.
10. Wan, J.; Xie, J.; Kong, X.; Liu, Z.; Liu, K.; Shi, F.; Pei, A.; Chen, H.; Chen, W.; Chen, J.; Zhang, X.; Zong, L.; Wang, J.; Chen, L. Q.; Qin, J.; Cui, Y., Ultrathin, flexible, solid polymer composite electrolyte enabled with aligned nanoporous host for lithium batteries. *Nat Nanotechnol* **2019,** *14* (7), 705-711.
11. Sheng, O.; Jin, C.; Luo, J.; Yuan, H.; Huang, H.; Gan, Y.; Zhang, J.; Xia, Y.; Liang, C.; Zhang, W.; Tao, X., $Mg_2B_2O_5$ Nanowire Enabled Multifunctional Solid-State Electrolytes with High Ionic Conductivity, Excellent Mechanical Properties, and Flame-Retardant Performance. *Nano Lett* **2018,** *18* (5), 3104-3112.
12. Liu, L.; Lyu, J.; Mo, J.; Yan, H.; Xu, L.; Peng, P.; Li, J.; Jiang, B.; Chu, L.; Li, M., Comprehensively-upgraded polymer electrolytes by multifunctional aramid nanofibers for stable all-solid-state Li-ion batteries. *Nano Energy* **2020,** *69*.
13. Chen, H.; Adekoya, D.; Hencz, L.; Ma, J.; Chen, S.; Yan, C.; Zhao, H.; Cui, G.; Zhang, S., Stable Seamless Interfaces and Rapid Ionic Conductivity of Ca–

CeO_2/LiTFSI/PEO Composite Electrolyte for High-Rate and High-Voltage All-Solid-State Battery. *Advanced Energy Materials* **2020,** *10* (21).
14. Lin, D.; Yuen, P. Y.; Liu, Y.; Liu, W.; Liu, N.; Dauskardt, R. H.; Cui, Y., A Silica-Aerogel-Reinforced Composite Polymer Electrolyte with High Ionic Conductivity and High Modulus. *Adv Mater* **2018,** *30* (32), e1802661.
15. Lin, D.; Liu, W.; Liu, Y.; Lee, H. R.; Hsu, P. C.; Liu, K.; Cui, Y., High Ionic Conductivity of Composite Solid Polymer Electrolyte via In Situ Synthesis of Monodispersed SiO_2 Nanospheres in Poly(ethylene oxide). *Nano Lett* **2016,** *16* (1), 459-65.
16. Li, Y.; Sun, Z.; Liu, D.; Gao, Y.; Wang, Y.; Bu, H.; Li, M.; Zhang, Y.; Gao, G.; Ding, S., A composite solid polymer electrolyte incorporating MnO_2 nanosheets with reinforced mechanical properties and electrochemical stability for lithium metal batteries. *Journal of Materials Chemistry A* **2020,** *8* (4), 2021-2032.
17. Li, Y.; Zhang, L.; Sun, Z.; Gao, G.; Lu, S.; Zhu, M.; Zhang, Y.; Jia, Z.; Xiao, C.; Bu, H.; Xi, K.; Ding, S., Hexagonal boron nitride induces anion trapping in a polyethylene oxide based solid polymer electrolyte for lithium dendrite inhibition. *Journal of Materials Chemistry A* **2020,** *8* (19), 9579-9589.
18. Zhang, J.; Zhao, N.; Zhang, M.; Li, Y.; Chu, P. K.; Guo, X.; Di, Z.; Wang, X.; Li, H., Flexible and ion-conducting membrane electrolytes for solid-state lithium batteries: Dispersion of garnet nanoparticles in insulating polyethylene oxide. *Nano Energy* **2016,** *28*, 447-454.
19. Zhao, Y.; Huang, Z.; Chen, S.; Chen, B.; Yang, J.; Zhang, Q.; Ding, F.; Chen, Y.; Xu, X., A promising PEO/LAGP hybrid electrolyte prepared by a simple method for all-solid-state lithium batteries. *Solid State Ionics* **2016,** *295*, 65-71.
20. Chen, L.; Li, Y.; Li, S.-P.; Fan, L.-Z.; Nan, C.-W.; Goodenough, J. B., PEO/garnet composite electrolytes for solid-state lithium batteries: From "ceramic-in-polymer" to "polymer-in-ceramic". *Nano Energy* **2018,** *46*, 176-184.
21. Li, D.; Chen, L.; Wang, T.; Fan, L. Z., 3D Fiber-Network-Reinforced Bicontinuous Composite Solid Electrolyte for Dendrite-free Lithium Metal Batteries. *ACS Appl Mater Interfaces* **2018,** *10* (8), 7069-7078.
22. Liu, W.; Liu, N.; Sun, J.; Hsu, P. C.; Li, Y.; Lee, H. W.; Cui, Y., Ionic conductivity enhancement of polymer electrolytes with ceramic nanowire fillers. *Nano Lett* **2015,** *15* (4), 2740-5.
23. Zhu, P.; Yan, C.; Dirican, M.; Zhu, J.; Zang, J.; Selvan, R. K.; Chung, C.-C.; Jia, H.; Li, Y.; Kiyak, Y.; Wu, N.; Zhang, X., $Li_{0.33}La_{0.557}TiO_3$ ceramic nanofiber-enhanced polyethylene oxide-based composite polymer electrolytes for all-solid-state lithium batteries. *Journal of Materials Chemistry A* **2018,** *6* (10), 4279-4285.